



KCC2-dependent Steady-state Intracellular Chloride Concentration and pH in Cortical Layer 2/3 Neurons of Anesthetized and Awake Mice

Juan C. Boffi^{*†}, Johannes Knabbe[†], Michaela Kaiser and Thomas Kuner

Department of Functional Neuroanatomy, Institute for Anatomy and Cell Biology, University of Heidelberg, Heidelberg, Germany

OPEN ACCESS

Edited by:

Claudio Rivera,
Aix-Marseille University, France

Reviewed by:

Stephen Moss,
Tufts University School of Medicine,
United States
Daniele Arosio,
Consiglio Nazionale delle Ricerche
(CNR), Italy

*Correspondence:

Juan C. Boffi
boffi@ana.uni-heidelberg.de

[†]These authors have contributed
equally to this work.

Received: 19 September 2017

Accepted: 05 January 2018

Published: 25 January 2018

Citation:

Boffi JC, Knabbe J, Kaiser M and
Kuner T (2018) KCC2-dependent
Steady-state Intracellular Chloride
Concentration and pH in Cortical
Layer 2/3 Neurons of Anesthetized
and Awake Mice.
Front. Cell. Neurosci. 12:7.
doi: 10.3389/fncel.2018.00007

Neuronal intracellular Cl^- concentration ($[\text{Cl}^-]_i$) influences a wide range of processes such as neuronal inhibition, membrane potential dynamics, intracellular pH (pH_i) or cell volume. Up to date, neuronal $[\text{Cl}^-]_i$ has predominantly been studied in model systems of reduced complexity. Here, we implemented the genetically encoded ratiometric Cl^- indicator Superclomeleon (SCLM) to estimate the steady-state $[\text{Cl}^-]_i$ in cortical neurons from anesthetized and awake mice using 2-photon microscopy. Additionally, we implemented superecliptic pHluorin (SE-pHluorin) as a ratiometric sensor to estimate the intracellular steady-state pH (pH_i) of mouse cortical neurons *in vivo*. We estimated an average resting $[\text{Cl}^-]_i$ of 6 ± 2 mM with no evidence of subcellular gradients in the proximal somato-dendritic domain and an average somatic pH_i of 7.1 ± 0.2 . Neither $[\text{Cl}^-]_i$ nor pH_i were affected by isoflurane anesthesia. We deleted the cation- Cl^- co-transporter KCC2 in single identified neurons of adult mice and found an increase of $[\text{Cl}^-]_i$ to approximately 26 ± 8 mM, demonstrating that under *in vivo* conditions KCC2 produces low $[\text{Cl}^-]_i$ in adult mouse neurons. In summary, neurons of the brain of awake adult mice exhibit a low and evenly distributed $[\text{Cl}^-]_i$ in the proximal somato-dendritic compartment that is independent of anesthesia and requires KCC2 expression for its maintenance.

Keywords: neuronal, intracellular, chloride, pH, *in vivo*, ratiometric imaging

INTRODUCTION

Neuronal $[\text{Cl}^-]_i$ is of crucial importance for processes such as inhibitory neurotransmission, maintenance of the resting membrane potential, regulation of intracellular pH (pH_i) and cell volume (Kaila et al., 2014; Doyon et al., 2016). This work is an attempt to gain insight into mammalian neuronal $[\text{Cl}^-]_i$ *in vivo* and thus contribute to the current knowledge in this field, which stems mainly from *in vitro* experiments. Although invaluable ground breaking work about neuronal $[\text{Cl}^-]_i$ has been produced *in vitro* (Delpire, 2000; Ben-Ari, 2002; Kaila et al., 2014), many factors inherent to routine *in vitro* preparations such as brain slices may influence $[\text{Cl}^-]_i$ regulation (Dzhala et al., 2012). Recent pioneering work achieved *in vivo* measurements of bulk tissue Cl^- dynamics (Wimmer et al., 2015; Berglund et al., 2016; Wells et al., 2016), but presently we know

Abbreviations: SCLM, Superclomeleon; SE-pHluorin, Superecliptic pHluorin.

very little about the *in vivo* steady-state neuronal [Cl⁻]_i and the factors affecting it (Bregestovski et al., 2009; Arosio and Ratto, 2014; Kaila et al., 2014; Doyon et al., 2016). Clomeleon was the first genetically encoded sensor to measure intracellular Cl⁻ and consists of a CFP-YFP pair in which the YFP FRET-acceptor is the Cl⁻ sensitive variant Topaz (Kuner and Augustine, 2000). However, the original version of Clomeleon has a Cl⁻ affinity of ~160 mM that is out of the expected physiological neuronal [Cl⁻]_i and a limited signal to noise ratio (Grimley et al., 2013). This led to the development of a second generation of promising genetically encoded Cl⁻ indicators with improved affinity and signal to noise ratio that could be used for *in vivo* applications, such as ClopHensor (Arosio et al., 2010) and Superclomeleon (SCLM; Grimley et al., 2013).

The affinity of most Cl⁻ sensitive fluorescent proteins for Cl⁻ is highly dependent on pH (Arosio et al., 2010; Grimley et al., 2013; Arosio and Ratto, 2014), which demands monitoring the cellular pH to validate the Cl⁻ readings made with these indicators. The design of ClopHensor-based sensors allows for simultaneous ratiometric pH and Cl⁻ measurements, but at the expense of being an excitation and emission ratiometric sensor. This hampers the *in vivo* implementation of ClopHensor-based sensors as its different excitation and emission wavelengths might be differentially scattered throughout the tissue at increasing imaging depths. While the present work was under review, a study by Sulis Sato et al. (2017) reported simultaneous *in vivo* optical estimations of neuronal Cl⁻ and pH in anesthetized mice using an optimized version of ClopHensor. The strong depth-dependent differential light scattering of the different wavelengths was compensated for by an offline correction algorithm. SCLM is not exempt of differential depth-dependent light scattering, but as it is an emission only ratiometric sensor instead, it might produce measurements less influenced by light scattering. This is at the expense of the need to monitor pH_i by other means.

Although neuronal pH has been studied *in vivo* using techniques such as nuclear magnetic resonance (Vorstrup et al., 1989), up to date mammalian neuronal pH_i has not been studied with cellular resolution *in vivo*. The use of a genetically encoded ratiometric fluorescent indicator is again a promising alternative to achieve this. Recently, the implementation of superecliptic (SE) pHluorin (Miesenböck et al., 1998) as an emission ratiometric pH indicator to monitor neuronal pH_i has been reported in flies (Rossano et al., 2013). This suggests a strategy combining ratiometric SCLM and superecliptic pHluorin (SE-pHluorin) recordings as a promising alternative to study neuronal steady-state Cl⁻ and pH *in vivo* using 2-photon microscopy.

Thus, to contribute to the on-going *in vivo* implementation of Cl⁻ imaging we established *in vivo* 2-photon microscopy in mice expressing SCLM or SE-pHluorin and explored the strengths and caveats of this ratiometric *in vivo* imaging approach. To gain insight into the factors affecting neuronal intracellular steady-state Cl⁻ concentration, we compared [Cl⁻]_i and pH_i in anesthetized and awake mice as well as in single neurons lacking the cation-Cl⁻ co-transporter KCC2 (Delpire, 2000; Ben-Ari, 2002; Kaila et al., 2014). These results and approach

will contribute to future studies of the role of Cl⁻ regulation in pathophysiological conditions such as epilepsy or schizophrenia *in vivo* (Kaila et al., 2014; Sullivan et al., 2015).

MATERIALS AND METHODS

Ethics Statement

This study was carried out in accordance with the European Communities Council Directive (86/609/EEC) to minimize animal pain or discomfort. All experiments were conducted following the German animal welfare guidelines specified in the TierSchG. The local animal care and use committee (Regierungspräsidium Karlsruhe of the state Baden-Württemberg) gave approval for the study under the number G183/15.

Animals

Experiments were performed on wild type (WT) or homozygous knock-in mice bearing floxed KCC2 alleles. The mouse strains used were C57Bl6N/CR and KCC2^{lox/lox} (Seja et al., 2012; Gödde et al., 2016). The latter mouse line was provided by Prof. Dr. Thomas Jensch (FMP/MDC, Berlin). All animals were 3–4 months of age by completion of data collection. Mice were housed up to three per cage and kept on a 12/12 h light/dark cycle. Food and water was available *ad libitum* except while the animals were restrained for imaging. Mice of either sex were used.

Genetically Encoded Indicators

The SCLM variant (Grimley et al., 2013) of Clomeleon (Kuner and Augustine, 2000) was used for non-invasive imaging of [Cl⁻]_i in layer 2/3 (L2/3) pyramidal cells of motor cortex. SCLM consists of the Cl⁻-insensitive Cerulean variant of green fluorescent protein connected by a linker to the Cl⁻-sensitive Topaz variant. The SE-pHluorin (Miesenböck et al., 1998) was used for pH_i estimations. The Cerulean-Venus tandem pair and EGFP were used as variants less sensitive to Cl⁻ and pH of SCLM and SE-pHluorin respectively, to evaluate imaging depth dependent scattering effects on ratiometric imaging. In all cases, expression in L2/3 pyramidal cells of motor cortex was driven by the Synapsin minimal promoter using a Cre-dependent DIO cassette. Plasmids encoding SCLM, SE-pHluorin, Venus and Cerulean were kind gifts of Prof. Dr. George Augustine (DukeNUS Medical School), Prof. Dr. Gero Miesenböck (University of Oxford), Dr. Atsushi Miyawaki (RIKEN) and Prof. Dr. Dave Piston (Vanderbilt University), respectively.

Calibration Curves

All calibrations were done *in vitro*, as *in vivo* calibration is not feasible because of the lack of control of local conditions. Calibration curves were constructed as described elsewhere (Grimley et al., 2013). Briefly, [Cl⁻]_i and pH in cultured hippocampal neurons expressing SCLM or SE-pHluorin were matched to those of the extracellular saline by treatment with ionophores: 10 μM nigericin and 5 μM tributyltin acetate (Alfa Aesar). Cells were perfused in the presence of ionophores

with calibration solutions of different $[\text{Cl}^-]$ or pH at a rate of 2 ml/min. High- $[\text{Cl}^-]$ calibration solution contained 105 mM KCl, 48 mM NaCl, 10 mM HEPES, 20 mM D(+)-glucose, 2 mM Na-EGTA and 4 mM MgCl_2 . Cl^- free calibration solution was composed of 10 mM HEPES, 20 mM D(+)-glucose, 48 mM Na-gluconate, 105 mM K-gluconate, 2 mM Na-EGTA, and 4 mM $\text{Mg}(\text{gluconate})_2$. Intermediate $[\text{Cl}^-]$ solutions were prepared by mixing these two solutions. The KF solution used to saturate SCLM contained 10 mM HEPES, 20 mM D(+)-glucose, 48 mM NaF, 105 mM KF, 2 mM Na-EGTA and 4 mM $\text{Mg}(\text{gluconate})_2$. For SCLM calibration curves, all salines were adjusted to pH 7.10 or pH 7.45. For SE-pHluorin calibration curves a calibration solution of 5 mM Cl^- was titrated to different pH values. Image acquisition started after 10 min. of incubation with the first calibration solution containing the ionophores and subsequent incubations were 6 min. each. Only a maximum of four incubations were performed per coverslip to avoid deterioration of the culture. SCLM calibration curves were constructed by fitting scatter plots of FRET ratios vs. $[\text{Cl}^-]$ to the equation $[\text{Cl}^-] = K_{d(\text{pH})}((R_{\text{max}} - R)/(R - R_{\text{min}}))(C_f/C_b)$ where $K_{d(\text{pH})}$ is the apparent dissociation constant at a given pH, R is the YFP/CFP emission ratio, R_{max} and R_{min} are the maximum and minimum ratios, C_f and C_b are the absolute CFP fluorescence values in the Cl^- free and fully bound state respectively (Grimley et al., 2013). Average R_{max} , R_{min} , C_f and C_b were determined experimentally for the fitting equation. SE-pHluorin calibration curves were constructed by fitting scatter plots of 530 nm/480 nm emission ratios to the Boltzmann equation (Rossano et al., 2013): $\text{pH} = R_{\text{min}} + (R_{\text{max}} - R_{\text{min}})/(1 + \exp((V50 - R)/n))$ where R is the 530 nm/480 nm emission ratio, R_{max} and R_{min} are the maximum and minimum ratios, $V50$ is the half maximum pH value and n is the slope.

Viral Vector Expression

Adeno-associated viral particles (AAV2/1-2 serotype) driving Cre recombinase expression, Cre-dependent or -independent expression of SCLM, SE-pHluorin, Cerulean-Venus or EGFP, all under the control of the Synapsin minimal promoter, were prepared for stereotaxic injections (Schwenger and Kuner, 2010). To achieve sparse but bright labeling of neurons that permitted the identification of each cell's projections, we co-injected AAVs encoding the Cre-dependent fluorescent proteins/sensors together with highly diluted (1/1000 to 1/5000) AAVs encoding nucleus-targeted Cre recombinase. Thus, due to the likelihood of the multiplicity of infection, very sparse but brightly labeled neurons could be imaged resolving their individual projections.

Stereotaxic Injection

For injection and craniectomy, mice were anesthetized by i.p. injection of a mixture of 40 μl fentanyl (1 mg/ml; Janssen), 160 μl midazolam (5 mg/ml; Hameln) and 60 μl medetomidin (1 mg/ml; Pfizer), dosed in 3.1 $\mu\text{l}/\text{g}$ body weight, placed in a stereotaxic headholder (Kopf) and a circular craniectomy (~ 7 mm) centered at bregma was made with a dental drill. The dura was carefully removed over the area for later injection with fine forceps cautiously avoiding damaging blood vessels. AAV particles were injected at L2/3 M1 motor cortex using the

following coordinates: in mm from the center of the craniectomy, considered bregma ($x; y$) = (1; 0). M1 cortex injections were performed using glass pipettes lowered to a depth of 300 μm to target L2/3. AAVs were injected using a syringe at a rate of ~ 1 $\mu\text{l}/\text{h}$. Volumes of virus of ~ 0.2 μl were injected per spot. All mutant mice used for virus injection were homozygous for the floxed KCC2 allele. A round 6 mm diameter number 0 coverslip (cranial window) disinfected with 70% ethanol and a custom made round plastic holder crown surrounding it for head fixation were cemented to the skull using dental acrylic (Hager and Werken). We targeted L2/3 of M1 cortex due to the accessibility of this cortical layer for 2P imaging and the convenience of the location over M1 cortex for hosting a 6 mm round cranial window, which allowed for multiple AAV injection sites thus refining our technique to reduce the number of animals needed for our experiments in conformity with our ethics statement. The skin wound around the window was also closed with dental acrylic. Mice received an i.p. mixture of 120 μl naloxon (0.4 mg/ml; Inresa), 800 μl flumazenil (0.1 mg/ml; Fresenius Kabi) and 60 μl antipamezole (5 mg/ml; Pfizer) dosed in 6.2 $\mu\text{l}/\text{g}$ body weight at the end of surgery to antagonize the anesthesia mix. Mice were given carprofen (Rimadyl, 5 mg/kg; Pfizer) as an analgesic immediately before surgery. Mice were single housed after surgery and typically imaged at least 28 days after virus injection and window implantation.

Two-Photon (2P) Imaging

2P imaging was done on a TriM Scope II microscope (LaVision BioTec GmbH) equipped with a pulsed Ti:Sapphire laser (Chameleon; Coherent). The light source was tuned to 840 nm for SCLM and Cerulean-Venus measurements or 810 nm for SE-pHluorin and EGFP measurements. Imaging was performed with a 25 \times , 1.1 numerical aperture, apochromatic, 2 mm working distance, water immersion objective (Nikon, MRD77225) and emitted fluorescence was split with a 495 nm dichroic, then filtered with 540/40 nm and 480/40 nm emission filters for SCLM and Cerulean-Venus measurements or 530/70 nm and 480/40 nm for SE-pHluorin or EGFP measurements (Chroma). Fluorescence emission was collected with low-noise high-sensitivity photomultiplier tubes (PMTs; Hamamatsu, H7422-40-LV 5M).

In Vivo 2P Imaging

For the imaging sessions of cranial window implanted mice, anesthesia was induced with 6% isoflurane (Baxter) in O_2 and maintained at 0.8%–1%. The anesthetized mouse was then head fixed on top of a rotating disc treadmill by a custom made head holder designed to fix a plastic holder crown surrounding the cranial window. This device was mounted onto the intravital stage of the 2P microscope. Fluorescence imaging in the anesthetized state was performed using line scanning. Typically, 16 bit frames of 491 μm^2 and 1024 px² resolution were acquired at a frame rate of 0.6 Hz and at 2 μm z steps. A full 3D stack spanning typically ~ 300 – 350 μm in depth took ~ 5 – 6 min. to acquire. Anesthetized imaging sessions lasted no longer than ~ 30 min. After the imaging session in the anesthetized state, the animal was allowed to

recover from anesthesia while still being head fixed at the microscope's stage (usually it took the mice 2–3 min to show clear signs of being awake such as to start whisking, blinking and walking). Throughout the imaging session the animal's breathing and behavior was monitored by means of an infra-red camera mounted to the stage while keeping the stage in the dark. After 5 min from withdrawal of isoflurane, awake imaging was performed under the aforementioned settings. Awake sessions (since the withdrawal of anesthesia) lasted no longer than ~15 min. After this the imaging session ended and the animal was returned to its cage.

In Vitro 2P Imaging

Hippocampal cultures were prepared from E16 rats according to established techniques (Kuner and Augustine, 2000). Infection of neuronal cultures with AAVs delivering the different expression constructs was performed on (DIV) 7–8. After virus infection and 4–7 day incubation for fluorescent protein expression, coverslips with cultured cells were transferred to a custom made perfusion chamber with temperature control mounted on the intravital stage of a triscope microscope (LaVision) equipped with a pulsed Ti:Sapphire laser (Chameleon; Coherent). All recordings were conducted at $35 \pm 2^\circ\text{C}$. Imaging was performed under the previously described settings. Except for calibration curves, hippocampal cultures were imaged in artificial cerebrospinal fluid (ACSF) gassed with carbogen (125 mM NaCl, 2.5 mM KCl, 25 mM NaHCO_3 , 1.25 NaH_2PO_4 , 1 mM MgCl_2 , 2 mM CaCl_2 , 25 mM D(+)-glucose, pH = 7.4). All chemicals were purchased from Sigma-Aldrich, except otherwise noted.

2P Imaging of Ratiometric Sensors

In a typical imaging session, the fluorescence emission collected at the shorter wavelength channel (cyan) was much weaker than the one from the longer wavelength channel (yellow/green). Hence, excitation laser power settings were optimized for cyan emission while avoiding saturation of the yellow/green emission channel, a compromise inherent to the dynamic range of ratiometric sensors based on CFP and YFP FRET pairs. To avoid “divided by background” ratio artifacts, we only analyzed regions of interest (ROIs) that exceeded the emission intensity of background twofold. For the sake of consistency, we only analyzed fluorescence ratios from cells with L2/3 pyramidal morphology, defined by the depth of the soma in the imaged volume, its size, shape and the presence of a marked apical dendrite (for simplicity referred to as pyramidal cells).

Analysis of Imaging Data

Image analysis was performed using Fiji (Schindelin et al., 2012) and data analysis and statistics were performed using Prism 7 software (GraphPad). ROIs spanning the cell somas, dendrites, dendritic spines or a cell-free background area were determined manually. Mean fluorescence intensity from each ROI were subtracted with the mean fluorescence intensity from the corresponding background area and background corrected fluorescence intensity ratios were calculated. Due to the low intensity emission registered for Cerulean and SE-pHluorin at

480 nm, only ROIs in which this fluorescence intensity was two-fold to that of the background were considered for further analysis.

Statistical Analyses

Normality was tested using Kolmogorov-Smirnov, D'Agostino-Pearson and Shapiro-Wilk tests. For paired samples with normally distributed frequencies, statistical significance was evaluated using paired *t*-tests. Wilcoxon tests were used for pairwise comparisons in which one or both samples were not normally distributed. For unpaired comparisons between highly variable samples, the whole frequency distributions were compared using Kolmogorov-Smirnov tests. Statistical differences to a theoretical value was evaluated using Wilcoxon signed rank tests. Variances of samples with different sizes were compared with Levene's test. Correlation was evaluated using the Pearson correlation coefficient. A $p < 0.05$ was considered significant.

RESULTS

In Vivo Imaging of SCLM-expressing Layer 2/3 Cortical Pyramidal Neurons in Anesthetized Mice

To explore the $[\text{Cl}^-]_i$ of neurons in the intact brain, we sparsely targeted SCLM expression to L2/3 of M1 cortex (**Figure 1A**), typically obtaining 1–20 neurons expressing SCLM in the entire mouse brain (see “Materials and Methods” section for details). Using this criterion 31 pyramidal cells were analyzed in dual color 3D stacks obtained from 5 head-fixed anesthetized WT mice. The Topaz component of SCLM gave rise to high fluorescence intensities even at depths of ~300 μm from the brain surface (**Figures 1A,B**), yet Cerulean fluorescence was lower. At low $[\text{Cl}^-]_i$, Topaz effectively acts as an acceptor for fluorescence resonance energy transfer from Cerulean, hence limiting the overall brightness of Cerulean fluorescence emission. To illustrate the signal strength over background of each emission channel rather than the intensity differences between the channels, both channels were clipped for display (**Figure 1**). In most neurons analyzed, a section of the apical dendrite of L2/3 pyramidal cells, proximal to the soma, consistently produced bright fluorescence in both emission channels that allowed reliable analysis. Regions with signal to background ratios of less than twofold were excluded for calculating the 540 nm/480 nm emission ratio (SCLM ratio), with high ratios representing low $[\text{Cl}^-]_i$ (**Figure 1B**).

A cell by cell pairwise comparison between the average SCLM ratio measured from a ROI spanning the soma or the apical dendrite of the 31 L2/3 pyramidal cells revealed no significant difference ($p = 0.3096$, paired *t*-test; **Figure 1B**), suggesting that intracellular Cl^- levels are rather homogeneous throughout these two subcellular compartments. Distal dendritic and spine $[\text{Cl}^-]_i$ could be imaged in some neurons (**Figure 1C**), nevertheless the lower signal to background ratio in these structures precluded a systematic analysis. Additionally, these few distal spiny dendritic stretches could not be traced back to

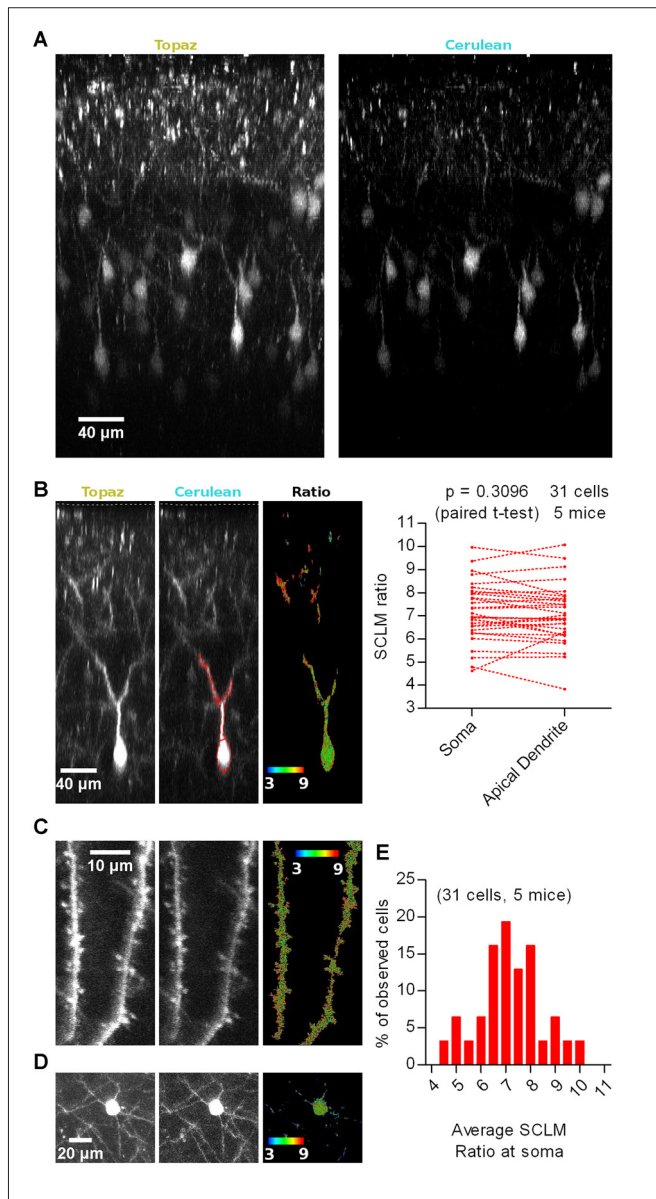


FIGURE 1 | *In vivo* imaging of Superclomeleon (SCLM)-expressing neurons in anesthetized mice. **(A)** Representative maximal intensity projections of a vertically resliced data stack showing the SCLM Topaz and Cerulean signal of sparsely labeled L2/3 neurons of M1 cortex in an anesthetized mouse. Gray values were clipped to include >90% of the total fluorescence signal: Topaz, 355–7996; Cerulean, 247–1390 **(B)** Left: representative maximal intensity projections of a vertically resliced data stack showing the *in vivo* SCLM Topaz and Cerulean signals and their corresponding ratio of a L2/3 pyramidal neuron from M1 cortex in an anesthetized mouse. For display, gray values were clipped to include >90% of the total fluorescence signal: Topaz, 291–4536; Cerulean, 111–757. The displayed neuron's soma centroid is $\sim 270 \mu\text{m}$ deep from the surface of the brain (included in the acquired stacks and marked with a white segmented line on the Topaz and Cerulean panels). Representative somatic and dendritic regions of interest (ROIs) enclosing areas with 2 fold signal to background emission intensities are displayed with red lines on the Cerulean panel. Right: pairwise comparison of the average SCLM 540 nm/480 nm emission ratio from ROIs spanning the basal apical dendrite and soma of L2/3 pyramidal neurons from M1 cortex in the anesthetized state. **(C)** Representative maximal intensity projections showing SCLM Topaz and Cerulean signals and their corresponding ratio of superficial spiny dendrites of L2/3 pyramidal neurons from M1 cortex in an anesthetized mouse. Gray values were clipped to include >90% of the total fluorescence signal: Topaz, 306–3655; Cerulean, 103–774. **(D)** Representative maximal intensity projections showing the *in vivo* SCLM Topaz and Cerulean signals and their corresponding ratio of the soma and basal dendrites of L2/3 pyramidal neurons from M1 cortex of an anesthetized mouse. Gray values were clipped to include >90% of the total fluorescence signal: Topaz, 90–2000; Cerulean, 96–295. **(E)** Histogram showing the frequency distribution of the recorded average SCLM 540 nm/480 nm emission ratio from ROIs spanning the somas of L2/3 pyramidal neurons from M1 cortex in the anesthetized state.

(Continued)

FIGURE 1 | Continued

Cerulean signals and their corresponding ratio of superficial spiny dendrites of L2/3 pyramidal neurons from M1 cortex in an anesthetized mouse. Gray values were clipped to include >90% of the total fluorescence signal: Topaz, 306–3655; Cerulean, 103–774. **(D)** Representative maximal intensity projections showing the *in vivo* SCLM Topaz and Cerulean signals and their corresponding ratio of the soma and basal dendrites of L2/3 pyramidal neurons from M1 cortex of an anesthetized mouse. Gray values were clipped to include >90% of the total fluorescence signal: Topaz, 90–2000; Cerulean, 96–295. **(E)** Histogram showing the frequency distribution of the recorded average SCLM 540 nm/480 nm emission ratio from ROIs spanning the somas of L2/3 pyramidal neurons from M1 cortex in the anesthetized state.

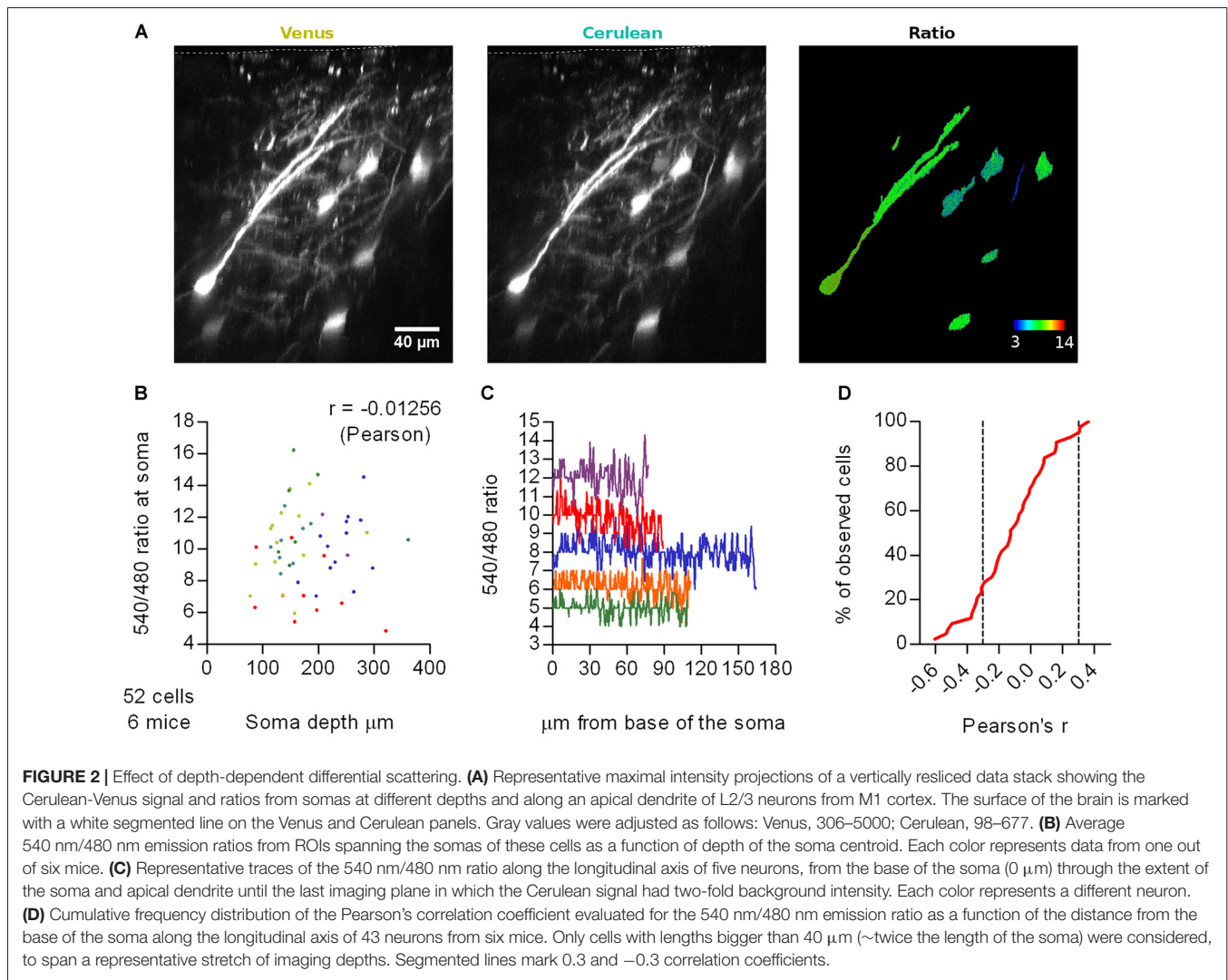
a cell soma. Similarly, the Cerulean fluorescence at the basal dendrites of L2/3 pyramidal cells was too low to produce reliable ratios (**Figure 1D**). These results suggest that $[\text{Cl}^-]_i$ would be evenly distributed within the proximal somato-dendritic domain up to $\sim 100 \mu\text{m}$ from the soma of L2/3 pyramidal neurons. Unfortunately, technical limitations do not allow measurements of $[\text{Cl}^-]_i$ in thin superficial dendrites and their spines as well as in thin basal dendrites deeper in the tissue.

We noticed that the fluorescence ratios differed substantially between individual neurons (**Figure 1E**). The large range of reported SCLM ratios could be a consequence of several factors: (1) depth-dependent differential scattering of the two emission wavelengths; (2) local *in vivo* imaging conditions (i.e., number of large blood vessels within the imaging pathway or other conditions of optical inhomogeneities); (3) biological variability, i.e., neurons having different resting $[\text{Cl}^-]_i$ or pH_i ; and (4) other factors. These issues will be addressed in following sections.

In summary, *in vivo* SCLM imaging with cellular resolution is feasible within cellular compartments that produce sufficiently high fluorescence intensity in the Cerulean emission channel at illumination intensities that do not saturate the Topaz channel, i.e., somata and thick dendrites of neurons. Within the proximal somato-dendritic domain spanning $\sim 100 \mu\text{m}$, $[\text{Cl}^-]_i$ would be evenly distributed with no detectable intracellular gradients in $[\text{Cl}^-]_i$.

Depth-Dependent Differential Scattering of Cyan and Yellow Fluorescence?

An intrinsic issue of ratiometric sensors is that their different emission wavelengths could be differentially scattered by the tissue, hence photons of different wavelengths emitted by SCLM traveling through different amounts of brain tissue at different imaging depths could produce depth-dependent artificial ratios. To address this problem, we designed an environmentally insensitive SCLM variant by replacing the Cl^- and pH sensitive Topaz yellow fluorescent protein with the reduced environmental sensitivity YFP variant Venus (Nagai et al., 2002). The pK_a value of Venus (6, Nagai et al., 2002) is slightly lower than that of SCLM (6.4, Grimley et al., 2013) and the K_d for Cl^- of Venus (10 M, Nagai et al., 2002) is strongly increased. Thus, Venus can be considered insensitive to Cl^- , yet slightly sensitive to pH. Cerulean is insensitive to pH in the range tested ($\text{pK}_a = 4.7$, Shaner et al., 2005) and its emission



is not influenced by Cl⁻ (Kuner and Augustine, 2000; Grimley et al., 2013). Hence, we replaced Topaz in SCLM with Venus, obtaining Cerulean-Venus. Thus, depth-dependent ratio changes would indicate differential scattering, while an invariant ratio would argue for depth-independence.

We sparsely expressed Cerulean-Venus in L2/3 pyramidal neurons of the motor cortex, under the same settings used with SCLM. We then recorded emission ratios at somas and apical dendrites at different imaging depths and included the surface of the brain in the image stack to estimate the depth of the somas (Figure 2A). *In vivo* 2P 3D stacks obtained from six head fixed anesthetized WT mice revealed that average somatic Cerulean-Venus ratios did not significantly correlate with the depth of the soma centroid (Pearson $r = -0.01256$, $p = 0.9296$, $n = 52$ cells; Figures 2A,B). To further assess the influence of light scattering in our measurements, we studied the emission ratio along the longitudinal axis of the neurons from the base of the soma towards the surface of the cortex along the apical dendrite until the most superficial position possible (Figure 2A, right panel). While individual

cells had rather different ratios, we could not find systematic shifts of the ratio along the dendritic tree (Figure 2C). We evaluated the correlation of the emission ratio vs. the distance along the longitudinal axis for each cell and found both positive and negative correlations (Figure 2D). The expected effect of scattering should manifest itself in only one sense of correlation, likely negative in this case due to higher scattering of shorter wavelengths. When analyzing this correlation in a cell by cell basis we found that 67% of the cells ($n = 52$) displayed Pearson correlation coefficients between -0.3 and 0.3, which could be considered weak or no correlation. Only in 26% of the cells, we observed coefficients lower than -0.3 and in 7% higher than 0.3. Thus, we conclude that differential depth-dependent scattering, within the range covered by our experiments, does not contaminate the ratiometric readout.

Similar to the ratios recorded with SCLM, Cerulean-Venus ratios displayed a pronounced dispersion when comparing different cells (Figure 2C). The observation that the ratios obtained with the environmentally much less sensitive

Cerulean-Venus and SCLM are dispersed in a similar fashion, suggests that the observed dispersion in SCLM ratios is not due to variation in intracellular $[\text{Cl}^-]_i$ between cells. This point will be further elaborated below.

In Vivo Ratiometric Imaging of SE-pHluorin-expressing Layer 2/3 Cortical Pyramidal Neurons

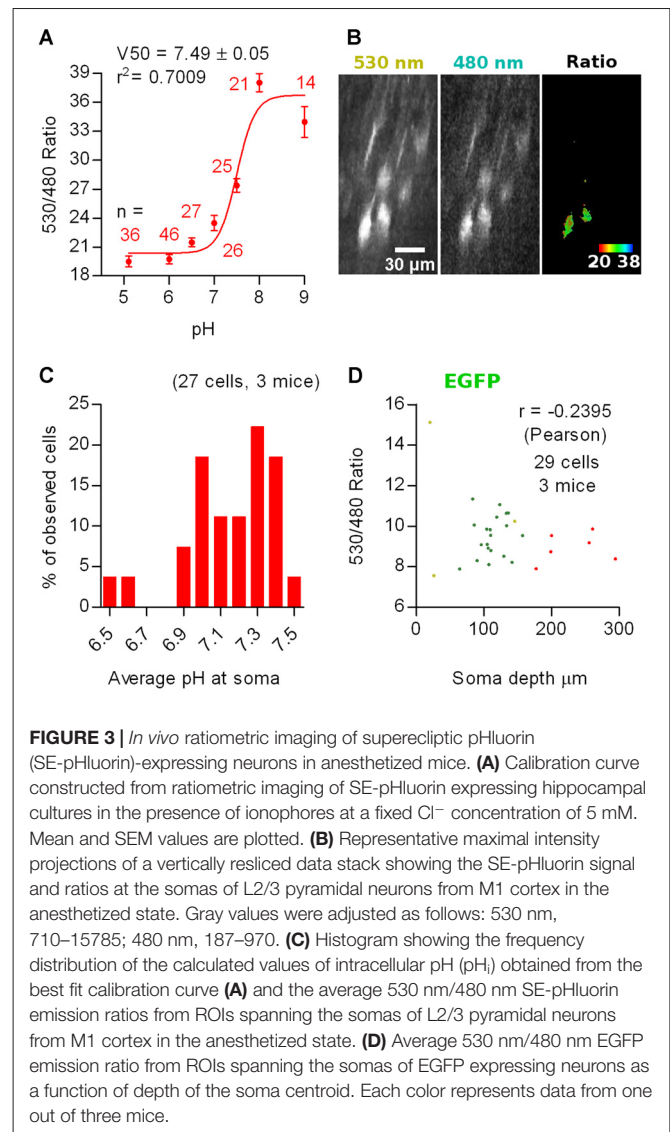
SCLM presents a sensitivity to pH that cannot be ignored as pH significantly affects the K_d of Cl^- for SCLM (Grimley et al., 2013). To determine the neuronal pH_i , we imaged L2/3 neurons of the motor cortex expressing SE-pHluorin. SE-pHluorin has been successfully used as a ratiometric pH indicator *in vitro* using excitation and emission wavelengths similar to those used for SCLM (Rossano et al., 2013), facilitating the implementation of this sensor for ratiometric pH estimations through minimal modifications to our method. SE-pHluorin was excited at 810 nm and 530 nm and 480 nm emission filters were used to calculate the 530 nm/480 nm ratio as a measure of pH_i (see “Materials and Methods” section).

To determine the average pH_i of the imaged cells, we constructed a calibration curve in SE-pHluorin-expressing hippocampal neuronal cultures by clamping pH_i to the extracellular saline by means of ionophore treatment at close to physiological temperature ($35 \pm 2^\circ\text{C}$). We fitted the data to the Boltzmann equation ($r^2 = 0.7009$) obtaining a best fit V_{50} value of 7.49 ± 0.05 (Figure 3A).

We sparsely expressed SE-pHluorin in superficial layers of motor cortex. Image stacks obtained from anesthetized mice revealed a similar compromise between the high intensity 530 nm emission and low intensity 480 nm emission as reported above for SCLM. In this case, the 480 nm emission at all processes including apical dendrites was too low to produce reliable ratios (double 480 nm emission than background fluorescence without saturating 530 nm emission). Consequently, we considered pyramidal cells having an oval/piriform soma with an extension representing the proximal portion of an apical dendrite. Thus, this *in vivo* imaging approach deep in intact brain tissue is limited to the somata of neurons and can not be used to assess pH_i in small compartments (Figure 3B).

Using the best fit parameters we calculated the pH_i corresponding to the average ratios recorded *in vivo* at the somas of 27 L2/3 pyramidal neurons from three mice. We found pH_i values ranging from 6.5 to 7.5 with a mean of 7.1 ± 0.2 (mean \pm 95% C.I., Figure 3C).

To rule out ratio artifacts due to imaging depth and differential scattering of the emission wavelengths, we repeated our experiments employing EGFP, which has reduced pH sensitivity ($\text{pK}_a = 6$, Shaner et al., 2005). We co-injected three mice with AAVs encoding Cre-dependent EGFP together with highly diluted Cre AAVs for bright and sparse labeling and repeated our measurements at L2/3 neurons using the same settings as with SE-pHluorin. We recorded somatic average emission ratios as a function of imaging depth. 3D stacks obtained from *in vivo* imaging sessions from three head fixed

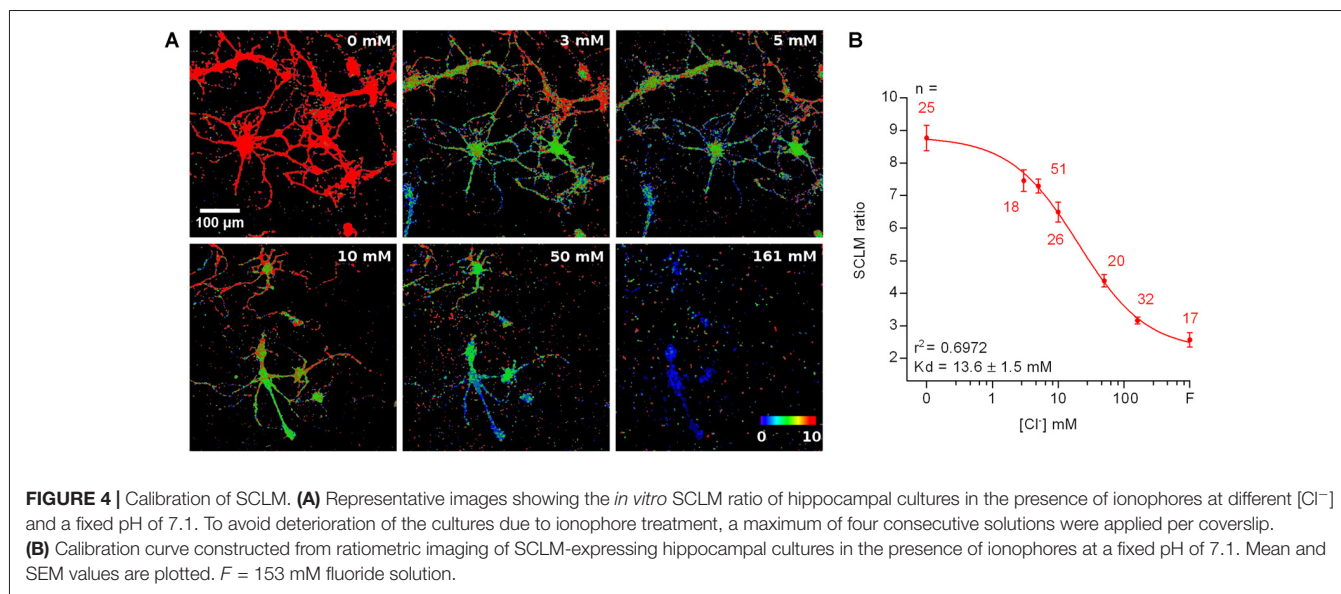


anesthetized WT mice revealed that the 530 nm/480 nm emission ratio of EGFP is not significantly correlated to the depth of the recorded soma in the tissue (Figure 3D). Hence, depth-dependent scattering in the emission wavelengths of SE-pHluorin is unlikely to affect our *in vivo* ratiometric pH estimations.

Interestingly, the ratios recorded with SE-pHluorin, displayed a pronounced dispersion that was significantly greater than those recorded with EGFP (for average somatic ratios, standard deviation: EGFP = 1.8, $n = 29$ cells; SE-pHluorin = 2.5, $n = 27$ cells; $p = 0.0010$, Levene’s test). This suggests that the observed dispersion in SE-pHluorin ratios is indicating an actual variation in pH_i between cells *in vivo*.

Calibration of SCLM and *in Vivo* $[\text{Cl}^-]_i$ Estimation

Ideally, pH_i and $[\text{Cl}^-]_i$ should be simultaneously determined in the same cellular compartment. However, SE-pHluorin imaging



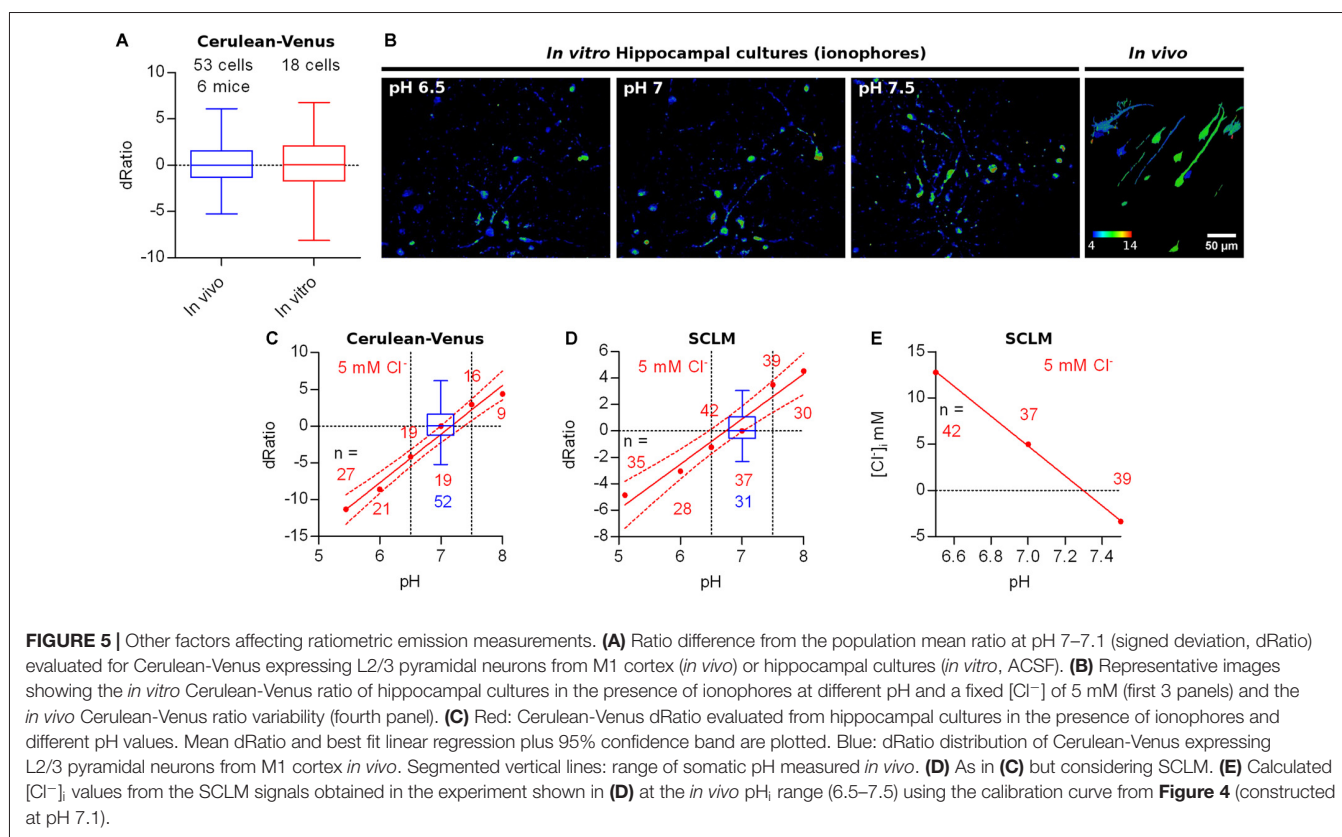
of neuronal pH_i is not compatible with simultaneous SCLM recordings. This means that it is not possible to calculate $[\text{Cl}^-]_i$ in a cell by cell basis from each cell's SCLM ratio at the corresponding pH_i . Hence, to estimate the average neuronal steady-state $[\text{Cl}^-]_i$ we constructed a calibration curve by clamping the $[\text{Cl}^-]_i$ and pH_i of SCLM-expressing hippocampal neurons to the extracellular saline through treatment with ionophores at a fixed pH corresponding to the average pH_i estimated *in vivo* ($\text{pH} = 7.1$, **Figure 4A**). To match physiological conditions we constructed this curve at near physiological temperature ($35 \pm 2^\circ\text{C}$). In these conditions our best fit value of K_d for Cl^- was 13.6 ± 1.5 mM ($r^2 = 0.6972$, **Figure 4B**). Using the best fit calibration curve, we estimated that the $[\text{Cl}^-]_i$ corresponding to the average SCLM ratio recorded *in vivo* at the somas of L2/3 pyramidal neurons of the motor cortex was 5 ± 2 mM in the anesthetized state (mean \pm 95% C.I.).

Other Factors Affecting Ratiometric Emission Measurements and Error Estimates Associated with pH Changes

As mentioned above, the observed variability in our ratiometric measurements could be explained by irregularities in the optical properties of the tissue (e.g., presence of blood vessels) at different parts of the volume imaged. To explore this possibility we compared the Cerulean-Venus emission ratios obtained *in vivo* from L2/3 cortical neurons to the ones observed *in vitro* in hippocampal neuronal cultures expressing Cerulean-Venus. Thus, neuronal cultures should be significantly less influenced by uneven optical properties as the cells would be more exposed than they would when located deep in intact brain tissue. We observed that the dispersion of Cerulean-Venus expressing cells *in vitro* and *in vivo* did not differ significantly (for average somatic ratios, standard deviation: *in vivo* = 2.4, $n = 52$ cells; *in vitro* = 3.5, $n = 18$ cells; $p = 0.1406$, Levene's test),

indicating that the variability in our ratiometric measurements was not caused by tissue inhomogeneity (**Figure 5A**), leaving pH_i differences between cells as a possible factor underlying this heterogeneity. To explore this further, we treated hippocampal cultures expressing Cerulean-Venus or SCLM with ionophores to manipulate their pH_i at a fixed $[\text{Cl}^-]$ of 5 mM and compared their ratios to our *in vivo* datasets (**Figure 5B**). To compare the variability in the ratios from these *in vitro* recordings at different pH_i to our *in vivo* datasets we evaluated the ratio difference from the population mean ratio (signed ratio deviation, dRatio) at pH_i 7 (*in vitro* dataset) or 7.1 (*in vivo* dataset). We compared the span of the best fit curve and the 95% confidence band from the Cerulean-Venus or SCLM dRatio as a function of pH_i , within the range of pH_i estimated *in vivo* (6.5–7.5), to the ratio deviation obtained from *in vivo* measurements. In doing so, we observed that the pH sensitivity of Cerulean-Venus or SCLM could account for practically all of the variability observed *in vivo* (**Figures 5C,D**).

Based on the quite pronounced variability of pH_i readouts, SCLM-expressing neurons may have a pH_i deviating from the average pH_i of 7.1, thereby introducing an error in the calculation of $[\text{Cl}^-]_i$ using the calibration curve constructed at the average *in vivo* pH_i . We estimated the extent of error introduced by this approach by using the SCLM calibration curve produced at pH 7.1 to calculate the $[\text{Cl}^-]_i$ corresponding to the ratios measured *in vitro* for **Figure 5D** within the *in vivo* estimated pH_i range (**Figure 3C**). Within this pH range (6.5–7.5), if we use the SCLM calibration curve performed at pH 7.1 to calculate the $[\text{Cl}^-]_i$ in a cell by cell basis, an error of up to ± 8 mM could be introduced to the $[\text{Cl}^-]_i$ (**Figure 5E**). Hence, this calibration approach using SCLM cannot accurately determine the $[\text{Cl}^-]_i$ in a cell by cell basis but it can estimate the $[\text{Cl}^-]_i$ of a hypothetical average cell with average pH_i . While the measurement error introduced with this approach will not suffice to resolve small changes in $[\text{Cl}^-]_i$, it might still be useful for experiments aimed at detecting larger changes in population $[\text{Cl}^-]_i$.



In Vivo Imaging of SCLM and SE-pHluorin-expressing Layer 2/3 Cortical Pyramidal Neurons in Awake Mice

The anesthetized condition generally involves increased GABAergic inhibition (Maciver, 2014). This could influence $[\text{Cl}^-]_i$, producing estimates that are not representative of the physiological awake state. We imaged SCLM-expressing neurons after initial isoflurane anesthesia in the awake state (**Figure 6A**). We performed again a cell by cell pairwise comparison between the average somatic SCLM ratio and the average apical dendritic ratio of 24 L2/3 pyramidal cells from five mice and observed no significant difference ($p = 0.5330$, Wilcoxon signed rank test; **Figure 6B**), suggesting that our previous observation about $[\text{Cl}^-]_i$ being homogeneous throughout these two subcellular compartments is not related to the anesthetized condition. Imaging in the awake state did not reveal significant differences in the distribution of somatic SCLM ratios ($p = 0.9120$, Kolmogorov-Smirnov; **Figure 6C**), indicating that the steady-state neuronal $[\text{Cl}^-]_i$ is not affected by isoflurane anesthesia and that SCLM ratios measured under anesthesia are representative of the awake state. A cell by cell pairwise comparison between the average somatic SCLM ratio recorded from 24 identified L2/3 pyramidal cells from five mice in the anesthetized and awake state showed no significant difference ($p = 0.6949$, paired t -test; **Figure 6D**), further supporting this notion.

To estimate $[\text{Cl}^-]_i$ in the awake state using a calibration curve, we first studied pH_i. Hence, we imaged SE-pHluorin in

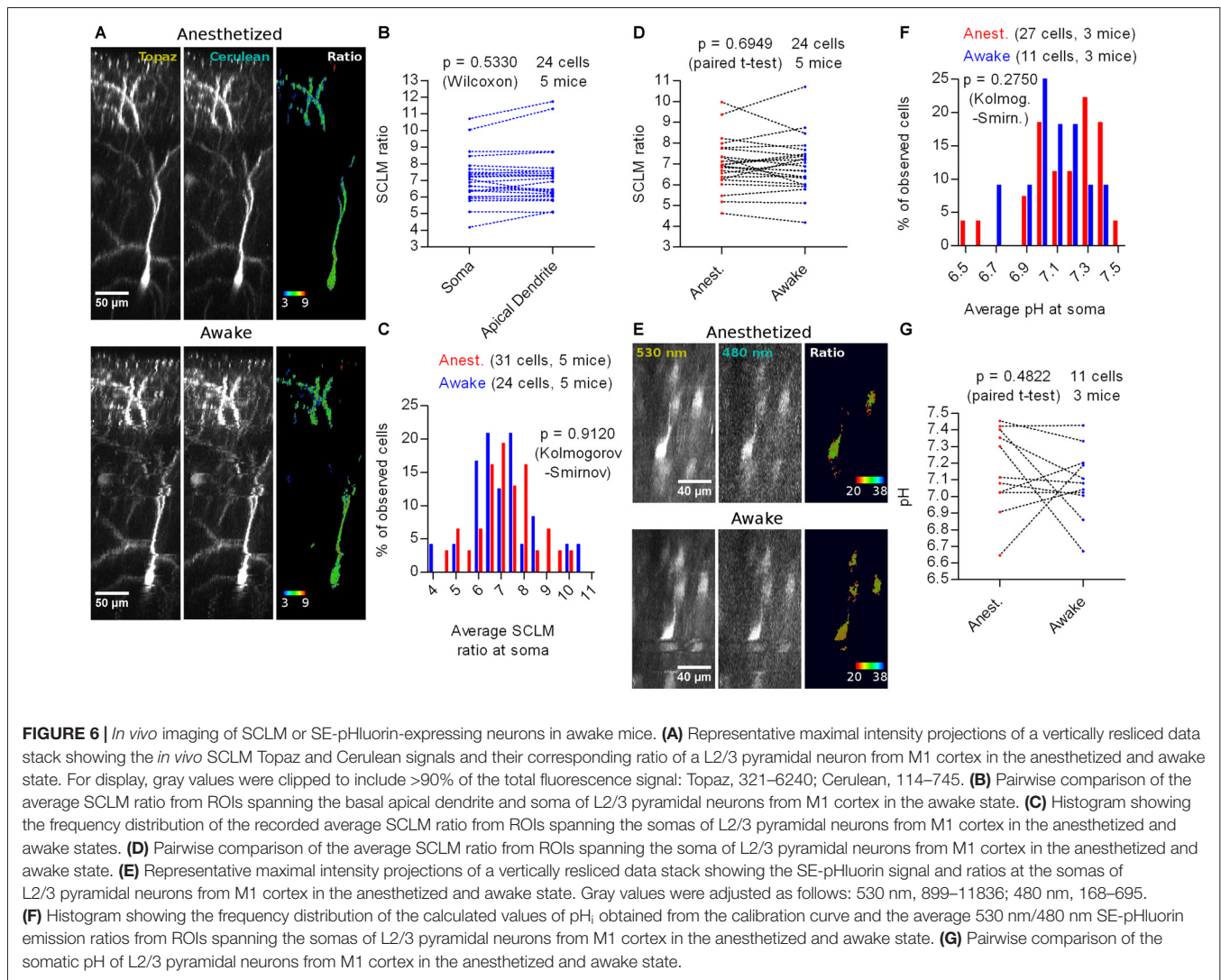
the awake state (**Figure 6E**) and found that the pH_i distribution is not significantly different to the one obtained under isoflurane anesthesia ($p = 0.2750$, Kolmogorov-Smirnov; **Figure 6F**). This result suggests that imaging SE-pHluorin under isoflurane anesthesia also does not produce artifactual measures of steady-state pH_i. A cell by cell pairwise comparison between the average somatic pH recorded from 11 identified L2/3 pyramidal cells from three mice in the anesthetized and awake state showed no significant difference ($p = 0.4822$, paired t -test; **Figure 6G**).

More importantly, these results suggest that the previous observation about the steady-state SCLM ratio being unaffected by anesthesia is truly reflecting a lack of effect on $[\text{Cl}^-]_i$. Using our best fit calibration curve (**Figure 4**), we estimated the $[\text{Cl}^-]_i$ using the average somatic SCLM ratio recorded *in vivo* in the awake state to be 6 ± 2 mM (mean \pm 95% C.I.).

To conclude, we did not find differences in $[\text{Cl}^-]_i$ or pH_i in cortical neurons of isoflurane anesthetized vs. awake mice, suggesting that steady-state $[\text{Cl}^-]_i$ or pH_i are not affected by isoflurane anesthesia.

In Vivo Effect of KCC2 Deletion on the Steady-state $[\text{Cl}^-]_i$ of Adult Layer 2/3 Cortex Neurons

As a proof of principle of our *in vivo* imaging approach and to explore the factors affecting the steady-state neuronal intracellular Cl^- *in vivo*, we co-injected AAVs encoding



Cre-dependent SCLM together with highly diluted AAVs encoding Cre recombinase into L2/3 of M1 cortex in adult $\text{KCC2}^{\text{lox/lox}}$ conditional KO mice (Seja et al., 2012; Gödde et al., 2016). Thus, expression of Cre recombinase will yield SCLM expression and abolish expression of KCC2. These mice were imaged at least 4 weeks after virus injection, which widely exceeds the reported KCC2 protein turnover time (Rivera et al., 2004). As a control for $[\text{Cl}^-]_i$ estimations, we injected AAVs encoding Cre-independent SCLM to assess $[\text{Cl}^-]_i$ in neurons of $\text{KCC2}^{\text{lox/lox}}$ mice without inducing the KO (from now on Ctrl cells). Additionally, to validate these measurements we determined the pH_i in Ctrl cells and KCC2 KO cells of $\text{KCC2}^{\text{lox/lox}}$ mice using SE-pHluorin and following the aforementioned approach (\pm Cre). The expression of Cre-independent SCLM and SE-pHluorin under the Synapsin promoter *in vivo* did not permit to distinguish pyramidal cell morphology as clearly as our Cre-dependent dilution approach, as the concomitant labeling of the tissue is much denser. Therefore, in these cases cells with clear pyramidal neuron

morphology were carefully selected for further analysis, thus discarding the great majority of labeled cells.

In vivo imaging of SE-pHluorin labeled KCC2 KO and Ctrl cells from six $\text{KCC2}^{\text{lox/lox}}$ mice showed that the KO did not affect the pH_i distribution (Anesthetized: $p = 0.0990$; Awake: $p = 0.2980$; Kolmogorov-Smirnov; **Figure 7A**). Again, we confirmed in the $\text{KCC2}^{\text{lox/lox}}$ genetic background, that isoflurane anesthesia does not affect the steady-state neuronal pH_i distribution (+Cre: $p = 0.8180$; –Cre: $p = 0.2710$; Kolmogorov-Smirnov; **Figure 7A**).

In vivo imaging of SCLM-labeled KCC2 KO cells from six mice showed significantly different average somatic SCLM ratio distributions than Ctrl (–Cre) cells from three mice (Anesthetized: $p < 0.0001$; Awake: $p < 0.0001$; Kolmogorov-Smirnov; **Figures 7B,C**). Once again, we observed no significant effect of isoflurane anesthesia in the SCLM ratio distributions from $\text{KCC2}^{\text{lox/lox}}$ mice, further supporting that isoflurane does not affect the distribution of steady-state neuronal $[\text{Cl}^-]_i$ (+Cre: $p = 0.6650$; –Cre: $p = 0.8600$; Kolmogorov-Smirnov;

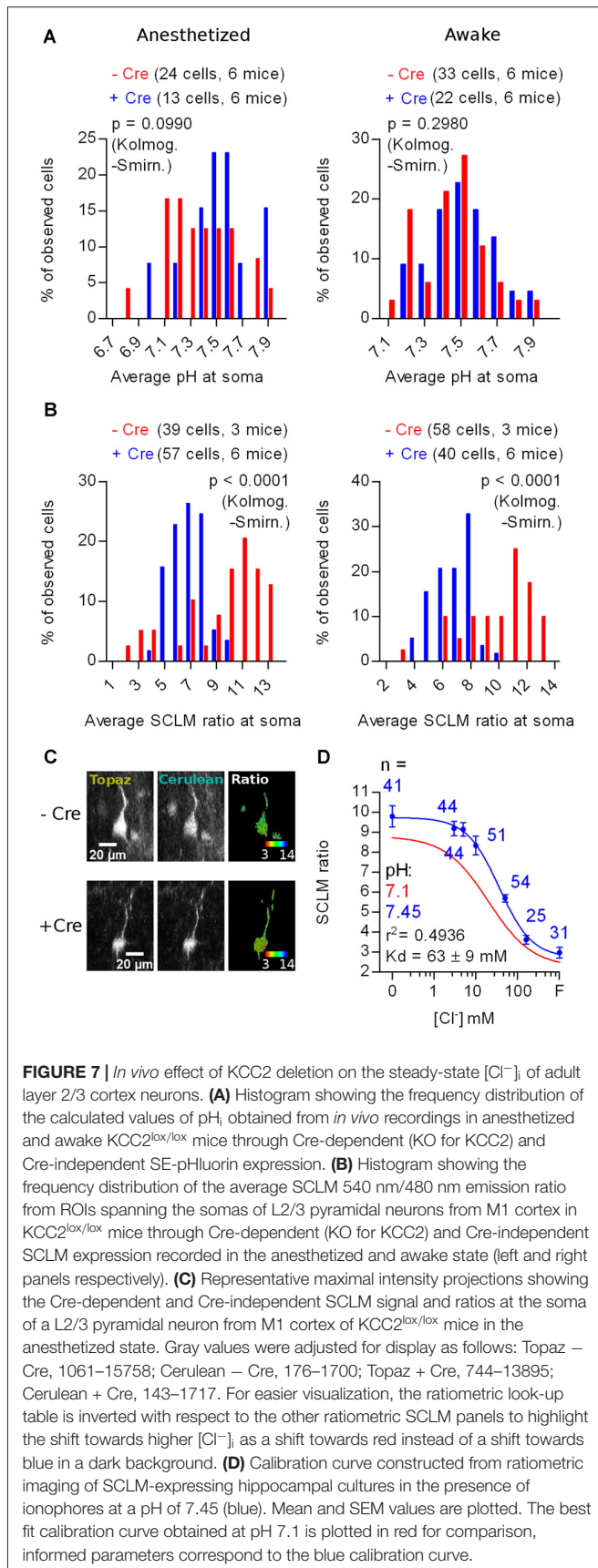


Figure 7B). The observed lack of change in the pH_i distribution (**Figure 7A**) confirms that the observed changes in the SCLM ratio distribution induced by deleting KCC2 (**Figure 7B**) are caused by changes in the steady-state neuronal $[\text{Cl}^-]_i$. Altogether, these results point out that the KO of KCC2 produces a shift towards lower SCLM ratios, which represent higher neuronal $[\text{Cl}^-]_i$ and that this effect is discernible *in vivo* using SCLM.

To calculate an estimate of the change in the average neuronal steady-state $[\text{Cl}^-]_i$, we constructed an *in vitro* calibration curve as previously described. We chose to produce this calibration curve at pH 7.45 because this value was not significantly different to the mean pH_i recorded in KCC2 KO cells from KCC2^{lox/lox} mice in both anesthetized or awake conditions (Anesthetized: $p = 0.2163$; Awake: $p = 0.1941$; Wilcoxon signed rank test). Thus, we used this single calibration curve produced at pH 7.45 to calculate estimates of the steady-state $[\text{Cl}^-]_i$ from the mean SCLM ratios recorded *in vivo* at the somas of KCC2 KO cells. This calibration curve showed a higher maximum ratio and K_d than the one produced at pH 7.1 (**Figure 7D**). The resulting steady-state $[\text{Cl}^-]_i$ estimation produced by KCC2 KO was $24.2 \pm 8 \text{ mM}$ in the anesthetized state and $25.7 \pm 8 \text{ mM}$ in the awake state (mean \pm 95% C.I.). In summary, KCC2 deletion produced a higher neuronal $[\text{Cl}^-]_i$, demonstrating a requirement of KCC2 for low $[\text{Cl}^-]_i$ in the adult mouse brain. Furthermore, these results indicate that effects in the magnitude of the changes reported here can be detected by *in vivo* SCLM imaging.

DISCUSSION

Our study reports non-invasive *in vivo* steady-state $[\text{Cl}^-]_i$ and pH_i estimations in L2/3 cortical neurons of anesthetized and awake mice. Independently of anesthesia, we estimated a native steady-state neuronal $[\text{Cl}^-]_i$ of $6 \pm 2 \text{ mM}$ which is consistent with numerous *in vitro* reports (Berglund et al., 2008; Bregestovski et al., 2009; Raimondo et al., 2013). According to the Nernst equation, a 6 mM steady-state neuronal $[\text{Cl}^-]_i$ paired with the expected extracellular $[\text{Cl}^-]$ (145 mM; Raimondo et al., 2015) would produce an E_{Cl} of $\sim(-85 \text{ mV})$ at 37°C , which is compatible with the expected values of healthy adult neurons (Doyon et al., 2016). If the Goldman equation is used to calculate the respective GABA_AR E_{rev} using the reported $[\text{Cl}^-]_i$ and the expected $[\text{HCO}_3^-]_i$ (15 mM) at the reported average pH_i , paired with the expected extracellular $[\text{Cl}^-]$ (145 mM) and $[\text{HCO}_3^-]$ (24 mM) concentrations (Raimondo et al., 2015) and a 4:1 permeability ratio for these two anions (Bormann et al., 1987), an E_{rev} of $\sim(-73 \text{ mV})$ is obtained, consistent with previously reported values (Kaila et al., 1993; Lee et al., 2015). This GABA_A E_{rev} could support hyperpolarizing inhibition, although the driving force at typical resting membrane potentials would be rather small. Therefore, Cl^- conductances will tend to produce shunting inhibition *in vivo*. Hence our results demonstrate that somatic steady-state $[\text{Cl}^-]_i$ determined *in vitro* can, in principle, be extrapolated to the native state found in the awake brain.

In this study we did not find evidence of differences in neuronal $[\text{Cl}^-]_i$ along the soma to proximal regions of the apical dendrite of cortical L2/3 pyramidal neurons. This is in contrast to *in vitro* reports studying other cell types such as cultured hippocampal or spinal cord neurons and retinal bipolar cells where clear somato-dendritic gradients were detected (Kuner and Augustine, 2000; Duebel et al., 2006; Waseem et al., 2010). Thus, our study suggests that within these subcellular compartments GABAergic inputs would be homogeneously inhibitory. The work of Waseem et al. (2010) in cultured neurons reports a stark gradient in $[\text{Cl}^-]_i$ between the soma and proximal dendritic compartment within a $\sim 20 \mu\text{m}$ distance. Nevertheless, this observation can be influenced by the maturation stage of the cultured cells, limited neuron-glia interactions and other uncontrolled factors inherent to this *in vitro* preparation such as abnormal neuronal activity, which can affect cation- Cl^- co-transporter trafficking and activation (Kaila et al., 2014). In this respect our study undertakes the effort to keep the intact native conditions of brain tissue as close as possible to the physiological state to avoid these issues. Under these conditions, we did not find evidence of a $[\text{Cl}^-]_i$ gradient at the proximal portion (up to $\sim 100 \mu\text{m}$ away from the soma) of the apical dendrite of L2/3 pyramidal neurons.

We found a steady-state pH_i of 7.1 ± 0.2 at the neuronal soma which is consistent with *in vitro* reports (Caspers and Speckmann, 1972; Raimondo et al., 2012). Our *in vivo* estimations of neuronal pH_i suggest that individual L2/3 pyramidal neurons differ in pH_i across a large range, also consistent with *in vitro* reports (Schwieging and Boron, 1994; Ruffin et al., 2014) and a recent *in vivo* report (Sulis Sato et al., 2017). Neuronal activity can dynamically affect pH_i (Chesler and Kaila, 1992). Thus it is possible that cells with different activity levels would underlie the observed range in pH_i . We could not systematically explore the occurrence of gradients in pH_i along the somato-dendritic axis, which is necessary to validate our result suggesting homogeneous $[\text{Cl}^-]_i$ along this compartment. Nevertheless, the occurrence of simultaneous $[\text{Cl}^-]_i$ and pH_i gradients producing perfectly opposing effects on SCLM ratios is highly unlikely. This is supported by our observation that somato-dendritic pH gradients could not be detected with the Cl^- -insensitive but slightly pH -sensitive Cerulean-Venus protein that otherwise reported cell-to-cell differences in pH . In conclusion we found that under native conditions of the awake adult brain, pH_i differs between cells by a large margin.

We provide *in vivo* evidence of the essential role of KCC2 in producing low neuronal $[\text{Cl}^-]_i$ in adult mouse neurons (Kaila et al., 2014; Doyon et al., 2016). In doing so, we show that despite the limitations of the SCLM/SE-pHluorin based *in vivo* imaging approach, it could resolve changes in neuronal $[\text{Cl}^-]_i$ that would be compatible to the ones expected during the developmental shift in $[\text{Cl}^-]_i$ (Ben-Ari, 2002; Kaila et al., 2014). Thus, a plausible future perspective of this work would be to explore the developmental $[\text{Cl}^-]_i$ shift in different genetically defined neuronal populations. The KO of KCC2 is expected to impact neuronal activity as it is evidenced in reports using pharmacological inhibitors of KCC2 in primary neuronal

cultures, acute brain slices and *in vivo* (Sivakumaran et al., 2015). In consequence, this change in neuronal activity could affect pH_i (Chesler and Kaila, 1992). Nevertheless, the sparse AAV-driven Cre recombinase expression in $\text{KCC2}^{\text{lox/lox}}$ mice affects only a small subset of neurons in the cortex in contrast to the global network effect of pharmacological KCC2 inhibitors which leads to epileptiform activity. Hence, even though the Cl^- driven synaptic inputs to KCC2 KO neurons would likely cause excitation, the overall inputs to the neuron would not be as drastically enhanced as in an epileptiform event, consistent with the observed lack of effect of the KCC2 KO on pH_i . Nonetheless, further controls of neuronal activity in KCC2 KO and Ctrl cells should be produced to fully address this point in future research.

Finally, our study provides a foundation for future *in vivo* research employing Cl^- and pH imaging in healthy and diseased tissue. While this article was under review, Sulis Sato et al. (2017) published an *in vivo* simultaneous Cl^- and pH imaging study using ClopHensor. In the following paragraphs we briefly compare the results produced by both sensors and discuss their strengths and caveats. *In vivo* 2P imaging of SCLM or SE-pHluorin showed a modest subcellular resolution. The main factor limiting this is the restricted 2P illumination settings needed to excite SCLM without saturating the Topaz emission channel, still obtaining reliable signal to noise levels in the Cerulean channel. Shorter 2P excitation wavelengths (800 nm) did not significantly improve this (data not shown). Alternatively, changing the relative sensitivity of the PMTs or replacing Cerulean for the higher quantum yield variant Teal, dramatically reduced the dynamic range of SCLM, thus practically abolishing the ability to resolve different $[\text{Cl}^-]_i$ (data not shown). Hence, the settings reported here represent the best compromise we found, still allowing us to explore the subcellular steady-state $[\text{Cl}^-]_i$ between the soma and apical dendrite of pyramidal neurons. Sulis Sato et al. (2017) did not explore subcellular differences in $[\text{Cl}^-]_i$ and pH_i due to better signal-to-noise levels at the soma compared to the dendrites, implying a similar limitation of ClopHensor.

The approach we describe to produce ratiometric Cl^- and pH estimations is not affected by isoflurane anesthesia. The anesthetized condition generally involves increased GABAergic inhibition (Maciver, 2014) and can have profound effects on breathing which could potentially alter cellular pH homeostasis (Massey et al., 2015). In the case of isoflurane, it has been reported to significantly enhance GABAergic inhibition in rat hippocampal slices and to mask the chemosensitivity of pH/CO_2 sensitive serotonergic neurons of the medulla (Maciver, 2014; Massey et al., 2015). Despite these known effects of isoflurane, *in vivo* optical steady-state estimations of $[\text{Cl}^-]_i$ and pH_i in L2/3 pyramidal neurons using SCLM and SE-pHluorin are not significantly affected by this anesthetic. The study of Sulis Sato et al. (2017) found similar $[\text{Cl}^-]_i$ and pH_i under urethane anesthesia.

Our approach was also not affected by light scattering caused by tissue depth or uneven optical properties. The use of ratiometric sensors such as SCLM deep in scattering tissue is expected to be hampered by differential scattering of two spectrally different fluorescence emissions. This study was started

with such expectation in mind and fluorescence life time imaging (FLIM) of the SCLM donor (Cerulean) was employed to obtain a depth-independent readout. However, the changes in life time as a function of [Cl⁻] in *in vitro* calibration curves were too small in order to resolve changes of [Cl⁻] in the physiologically relevant range (data not shown). The emission ratio of an environmentally less sensitive construct, Cerulean-Venus, did not significantly change up to a depth of approximately 350–400 μm. Therefore, motor cortex, and possibly brain tissue in general, appears to scatter emission light in the range from 480 nm to 540 nm in a manner so similar that changes in the ratio as a function of depth were not evident, suggesting that this spectral range can be used for ratiometric recordings without applying complicated depth-dependent corrections. This is reported to be fundamentally different when ratiometric indicators using the green-red range of the emission spectrum are employed, such as ClopHensor, as brain tissue shows a strong depth-dependent differential scattering for this range of the spectrum (Sulis Sato et al., 2017). On the other hand excitation light of different wavelengths can be differentially scattered as a function of imaging depth producing “distortions” on the absorption spectra of fluorescent proteins (Sulis Sato et al., 2017). Nevertheless, our ratiometric imaging approach required only one excitation wavelength, making it relatively less prone to be affected by this issue in comparison to ClopHensor (Sulis Sato et al., 2017). Again, this is supported by the observed lack of correlation between the imaging depth and the recorded ratios for Cerulean-Venus or EGFP expressing neurons *in vivo*.

Additionally the presence of blood vessels and fiber bundles can make the optical properties of brain tissue inhomogeneous, which can also cause scattering artifacts. By comparing the Cerulean-Venus ratios recorded *in vivo* to the ones recorded in hippocampal cultures we demonstrated that our ratiometric approach is not significantly affected by this factor. Altogether, we provide evidence supporting that ratiometric imaging in the emission range from 480 nm to 540 nm is robust against these inherent scattering-related issues of ratiometric imaging in intact brain tissue, an insight that will be relevant for *in vivo* applications of a multitude of genetically encoded indicators employing the CFP-YFP FRET pair.

The use of SCLM for intracellular Cl⁻ estimations needs validation due to its pH sensitivity. Yet, simultaneous recordings

of pH_i and [Cl⁻]_i using this approach are technically not yet possible. The observed diverse range of neuronal pH_i makes SCLM readouts quite variable between individual cells. This is a major limitation in SCLM imaging that demands a compatible method to simultaneously measure pH_i and achieve calculations of [Cl⁻]_i for individual cells. Additionally, as neuronal activity also affects pH_i (Chesler and Kaila, 1992), this also stresses the need of simultaneous pH_i readouts to assess dynamic neuronal Cl⁻ changes using SCLM.

In conclusion, this report contributes to the study of neuronal [Cl⁻]_i and pH_i by providing estimations as close to the native state as practically possible. These results and approach represent a step forward towards the understanding of essential neuronal processes involving [Cl⁻]_i in the intact organism and aid in the quest to relieve pathophysiological conditions such as epilepsy or schizophrenia (Kaila et al., 2014; Sullivan et al., 2015).

AUTHOR CONTRIBUTIONS

JCB, JK and TK designed research, reviewed and edited the manuscript. MK designed and constructed expression plasmids. JCB and JK performed imaging experiments. JCB performed data analysis and prepared figures. JCB and TK wrote the manuscript.

ACKNOWLEDGMENTS

TK acknowledges funding by the CellNetworks Cluster of Excellence (EXC 81) and a large equipment grant by the Deutsche Forschungsgemeinschaft (DFG). We thank Prof. Dr. Thomas Jentsch, Prof. Dr. George Augustine, Prof. Dr. Gero Miesenböck, Prof. Dr. Dave Piston, Dr. Atsushi Miyawaki, Prof. Dr. Jochen Kuhse and Prof. Dr. Hilmar Bading for providing materials. We would also like to thank Dr. Christoph Körber and Dr. Patric Pelzer for helpful discussion and comments on the manuscript, Claudia Kocksch and Gabriela E. Krämer for technical assistance. We gratefully acknowledge the data storage service SDS@hd supported by the Ministry of Science, Research and the Arts Baden-Württemberg (MWK) and the German Research Foundation (DFG) through grant INST 35/1314-1 FUGG. We acknowledge the financial support of the Deutsche Forschungsgemeinschaft and Ruprecht-Karls-Universität Heidelberg within the funding program Open Access Publishing.

REFERENCES

- Arosio, D., and Ratto, G. M. (2014). Twenty years of fluorescence imaging of intracellular chloride. *Front. Cell. Neurosci.* 8:258. doi: 10.3389/fncel.2014.00258
- Arosio, D., Ricci, F., Marchetti, L., Gualdani, R., Albertazzi, L., and Beltram, F. (2010). Simultaneous intracellular chloride and pH measurements using a GFP-based sensor. *Nat. Methods* 7, 516–518. doi: 10.1038/nmeth.1471
- Ben-Ari, Y. (2002). Excitatory actions of gaba during development: the nature of the nurture. *Nat. Rev. Neurosci.* 3, 728–739. doi: 10.1038/nrn920
- Berglund, K., Schleich, W., Wang, H., Feng, G., Hall, W. C., Kuner, T., et al. (2008). Imaging synaptic inhibition throughout the brain via genetically targeted Clomeleon. *Brain Cell Biol.* 36, 101–118. doi: 10.1007/s11068-008-9031-x
- Berglund, K., Wen, L., Dunbar, R. L., Feng, G., and Augustine, G. J. (2016). Optogenetic visualization of presynaptic tonic inhibition of cerebellar parallel fibers. *J. Neurosci.* 36, 5709–5723. doi: 10.1523/JNEUROSCI.4366-15.2016
- Bormann, J., Hamill, O. P., and Sakmann, B. (1987). Mechanism of anion permeation through channels gated by glycine and γ-aminobutyric acid in mouse cultured spinal neurones. *J. Physiol.* 385, 243–286. doi: 10.1113/jphysiol.1987.sp016493
- Bregestovski, P., Waseem, T., and Mukhtarov, M. (2009). Genetically encoded optical sensors for monitoring of intracellular chloride and chloride-selective channel activity. *Front. Mol. Neurosci.* 2:15. doi: 10.3389/neuro.02.015.2009
- Caspers, H., and Speckmann, E. J. (1972). Cerebral pO₂, pCO₂ and pH: changes during convulsive activity and their significance for spontaneous arrest of seizures. *Epilepsia* 13, 699–725. doi: 10.1111/j.1528-1157.1972.tb04403.x

- Chesler, M., and Kaila, K. (1992). Modulation of pH by neuronal activity. *Trends Neurosci.* 15, 396–402. doi: 10.1016/0166-2236(92)90191-a
- Delpire, E. (2000). Cation-chloride cotransporters in neuronal communication. *News Physiol. Sci.* 15, 309–312. doi: 10.1152/physiologyonline.2000.15.6.309
- Doyon, N., Vinay, L., Prescott, S. A., and De Koninck, Y. (2016). Chloride regulation: a dynamic equilibrium crucial for synaptic inhibition. *Neuron* 89, 1157–1172. doi: 10.1016/j.neuron.2016.02.030
- Duebel, J., Haverkamp, S., Schleich, W., Feng, G., Augustine, G. J., Kuner, T., et al. (2006). Two-photon imaging reveals somatodendritic chloride gradient in retinal ON-type bipolar cells expressing the biosensor Clomeleon. *Neuron* 49, 81–94. doi: 10.1016/j.neuron.2005.10.035
- Dzhala, V., Valeeva, G., Glykys, J., Khazipov, R., and Staley, K. (2012). Traumatic alterations in GABA signaling disrupt hippocampal network activity in the developing brain. *J. Neurosci.* 32, 4017–4031. doi: 10.1523/JNEUROSCI.5139-11.2012
- Gödde, K., Gschwend, O., Puchkov, D., Pfeffer, C. K., Carleton, A., and Jentsch, T. J. (2016). Disruption of Kcc2-dependent inhibition of olfactory bulb output neurons suggests its importance in odour discrimination. *Nat. Commun.* 7:12043. doi: 10.1038/ncomms12043
- Grimley, J. S., Li, L., Wang, W., Wen, L., Beese, L. S., Hellinga, H. W., et al. (2013). Visualization of synaptic inhibition with an optogenetic sensor developed by cell-free protein engineering automation. *J. Neurosci.* 33, 16297–16309. doi: 10.1523/JNEUROSCI.4616-11.2013
- Kaila, K., Price, T. J., Payne, J. A., Puskarjov, M., and Voipio, J. (2014). Cation-chloride cotransporters in neuronal development, plasticity and disease. *Nat. Rev. Neurosci.* 15, 637–654. doi: 10.1038/nrn3819
- Kaila, K., Voipio, J., Paalasmaa, P., Pasternack, M., and Deisz, R. A. (1993). The role of bicarbonate in GABA_A receptor-mediated IPSPs of rat neocortical neurones. *J. Physiol.* 464, 273–289. doi: 10.1113/jphysiol.1993.sp019634
- Kuner, T., and Augustine, G. J. (2000). A genetically encoded ratiometric indicator for chloride: capturing chloride transients in cultured hippocampal neurons. *Neuron* 27, 447–459. doi: 10.1016/s0896-6273(00)00056-8
- Lee, S. W., Kim, Y. B., Kim, J. S., Kim, W. B., Kim, Y. S., Han, H. C., et al. (2015). GABAergic inhibition is weakened or converted into excitation in the oxytocin and vasopressin neurons of the lactating rat. *Mol. Brain* 8:34. doi: 10.1186/s13041-015-0123-0
- Maciver, M. B. (2014). Anesthetic agent-specific effects on synaptic inhibition. *Anesth. Analg.* 119, 558–569. doi: 10.1213/ANE.0000000000000321
- Massey, C. A., Iccaman, K. E., Johansen, S. L., Wu, Y., Harris, M. B., and Richerson, G. B. (2015). Isoflurane abolishes spontaneous firing of serotonin neurons and masks their pH/CO₂ chemosensitivity. *J. Neurophysiol.* 113, 2879–2888. doi: 10.1152/jn.01073.2014
- Miesenböck, G., De Angelis, D. A., and Rothman, J. E. (1998). Visualizing secretion and synaptic transmission with pH-sensitive green fluorescent proteins. *Nature* 394, 192–195. doi: 10.1038/28190
- Nagai, T., Ibata, K., Park, E. S., Kubota, M., Mikoshiba, K., and Miyawaki, A. (2002). A variant of yellow fluorescent protein with fast and efficient maturation for cell-biological applications. *Nat. Biotechnol.* 20, 87–90. doi: 10.1038/nbt0102-87
- Raimondo, J. V., Burman, R. J., Katz, A. A., and Akerman, C. J. (2015). Ion dynamics during seizures. *Front. Cell. Neurosci.* 9:419. doi: 10.3389/fncel.2015.00419
- Raimondo, J. V., Irtle, A., Wefelmeyer, W., Newey, S. E., and Akerman, C. J. (2012). Genetically encoded proton sensors reveal activity-dependent pH changes in neurons. *Front. Mol. Neurosci.* 5:68. doi: 10.3389/fnmol.2012.00068
- Raimondo, J. V., Joyce, B., Kay, L., Schlagheck, T., Newey, S. E., Srinivas, S., et al. (2013). A genetically-encoded chloride and pH sensor for dissociating ion dynamics in the nervous system. *Front. Cell. Neurosci.* 7:202. doi: 10.3389/fncel.2013.00202
- Rivera, C., Voipio, J., Thomas-Crusells, J., Li, H., Emri, Z., Sipilä, S., et al. (2004). Mechanism of activity-dependent downregulation of the neuron-specific K-Cl cotransporter KCC2. *J. Neurosci.* 24, 4683–4691. doi: 10.1523/JNEUROSCI.5265-03.2004
- Rossano, A. J., Chouhan, A. K., and Macleod, G. T. (2013). Genetically encoded pH-indicators reveal activity-dependent cytosolic acidification of *Drosophila* motor nerve termini *in vivo*. *J. Physiol.* 591, 1691–1706. doi: 10.1113/jphysiol.2012.248377
- Ruffin, V. A., Salameh, A. I., Boron, W. F., and Parker, M. D. (2014). Intracellular pH regulation by acid-base transporters in mammalian neurons. *Front. Physiol.* 5:43. doi: 10.3389/fphys.2014.00043
- Schindelin, J., Arganda-Carreras, I., Frise, E., Kaynig, V., Longair, M., Pietzsch, T., et al. (2012). Fiji: an open-source platform for biological-image analysis. *Nat. Methods* 9, 676–682. doi: 10.1038/nmeth.2019
- Schwenger, D. B., and Kuner, T. (2010). Acute genetic perturbation of exocyst function in the rat calyx of Held impedes structural maturation, but spares synaptic transmission. *Eur. J. Neurosci.* 32, 974–984. doi: 10.1111/j.1460-9568.2010.07391.x
- Schwiening, C. J., and Boron, W. F. (1994). Regulation of intracellular pH in pyramidal neurones from the rat hippocampus by Na(+)-dependent Cl(-)-HCO₃- exchange. *J. Physiol.* 475, 59–67. doi: 10.1113/jphysiol.1994.sp020049
- Seja, P., Schonewille, M., Spitzmaul, G., Badura, A., Klein, I., Rudhard, Y., et al. (2012). Raising cytosolic Cl⁻ in cerebellar granule cells affects their excitability and vestibulo-ocular learning. *EMBO J.* 31, 1217–1230. doi: 10.1038/emboj.2011.488
- Shaner, N. C., Steinbach, P. A., and Tsien, R. Y. (2005). A guide to choosing fluorescent proteins. *Nat. Methods* 2, 905–909. doi: 10.1038/nmeth819
- Sivakumaran, S., Cardarelli, R. A., Maguire, J., Kelley, M. R., Silayeva, L., Morrow, D. H., et al. (2015). Selective inhibition of KCC2 leads to hyperexcitability and epileptiform discharges in hippocampal slices and *in vivo*. *J. Neurosci.* 35, 8291–8296. doi: 10.1523/jneurosci.5205-14.2015
- Sulis Sato, S., Artoni, P., Landi, S., Cozzolino, O., Parra, R., Pracucci, E., et al. (2017). Simultaneous two-photon imaging of intracellular chloride concentration and pH in mouse pyramidal neurons *in vivo*. *Proc. Natl. Acad. Sci. U S A* 114, E8770–E8779. doi: 10.1073/pnas.1702861114
- Sullivan, C. R., Funk, A. J., Shan, D., Haroutunian, V., and Mccullumsmith, R. E. (2015). Decreased chloride channel expression in the dorsolateral prefrontal cortex in schizophrenia. *PLoS One* 10:e0123158. doi: 10.1371/journal.pone.0123158
- Vorstrup, S., Jensen, K. E., Thomsen, C., Henriksen, O., Lassen, N. A., and Paulson, O. B. (1989). Neuronal pH regulation: constant normal intracellular pH is maintained in brain during low extracellular pH induced by acetazolamide—³¹P NMR study. *J. Cereb. Blood Flow Metab.* 9, 417–421. doi: 10.1038/jcbfm.1989.61
- Waseem, T., Mukhtarov, M., Buldakova, S., Medina, I., and Bregestovski, P. (2010). Genetically encoded Cl-Sensor as a tool for monitoring of Cl-dependent processes in small neuronal compartments. *J. Neurosci. Methods* 193, 14–23. doi: 10.1016/j.jneumeth.2010.08.002
- Wells, M. F., Wimmer, R. D., Schmitt, L. I., Feng, G., and Halassa, M. M. (2016). Thalamic reticular impairment underlies attention deficit in Ptchd1(Y⁻) mice. *Nature* 532, 58–63. doi: 10.1038/nature17427
- Wimmer, R. D., Schmitt, L. I., Davidson, T. J., Nakajima, M., Deisseroth, K., and Halassa, M. M. (2015). Thalamic control of sensory selection in divided attention. *Nature* 526, 705–709. doi: 10.1038/nature15398

Conflict of Interest Statement: The authors declare that the research was conducted in the absence of any commercial or financial relationships that could be construed as a potential conflict of interest.

Copyright © 2018 Boffi, Knabbe, Kaiser and Kuner. This is an open-access article distributed under the terms of the Creative Commons Attribution License (CC BY). The use, distribution or reproduction in other forums is permitted, provided the original author(s) or licensor are credited and that the original publication in this journal is cited, in accordance with accepted academic practice. No use, distribution or reproduction is permitted which does not comply with these terms.